where K_2 is the adsorption equilibrium constant for excess TEA on adsorbed Cu(II)-TEA.

From Eq. [A-1] to [A-4], the fractional surface coverage of active Cu(II)-TEA is expressed as

$$\theta_3 = \frac{K_1 \cdot C_{xl}}{1 + K_1 \cdot C_{xl}} \cdot \frac{K_3 \cdot C_c}{1 + K_3 \cdot C_c} \cdot \frac{1}{1 + K_2 \cdot C_{xl}} \quad [1]$$

When the differential coefficient of Eq. [1] is equal to 0, the maximum fractional surface coverage can be defined as $\theta_{3,max}$. The differential equation of θ_3 by C_{xl} is

$$\frac{d(\theta_3)}{d(C_{xl})} = \frac{K_3 \cdot C_c}{1 + K_3 \cdot C_c} \cdot \frac{K_1 \cdot (1 - K_1 \cdot K_2 \cdot C_{xl}^2)}{(1 + K_1 \cdot C_{xl})^2 \cdot (1 + K_2 \cdot C_{xl})^2} = 0 \quad [A\text{-}5]$$

From Eq. [A-5] C_{xl} at $\theta_{3,max}$ is

$$C_{xl}(\theta_{max}) = \sqrt{\frac{1}{K_1 \cdot K_2}} \quad [A\text{-}6]$$

Therefore the maximum fractional surface coverage can be expressed as

$$\theta_{3,max} = \frac{K_3 \cdot C_c}{1 + K_3 \cdot C_c} \cdot \frac{1}{(1 + \sqrt{K_2/K_1})^2} \quad [2]$$

Since the deposition rate is proportional to the fractional surface coverage, the rate related to the concentration of excess TEA from Eq. [1] and [2] is expressed as

$$\frac{\theta_3}{\theta_{3,max}} = \frac{r}{r_{max}} = \left(1 + \sqrt{\frac{K_2}{K_1}}\right)^2 \cdot \frac{K_1 \cdot C_{xl}}{1 + K_1 \cdot C_{xl}} \cdot \frac{1}{1 + K_2 \cdot C_{xl}} \quad [3]$$

where r_{max} is the deposition rate at $\theta_{3,max}$, and r is the deposition rate measured at θ_3.

REFERENCES

1. L. N. Schoenberg, *This Journal*, **119**, 1491 (1972).
2. A. Hung, *ibid.*, **132**, 1047 (1985).
3. A. Hung, *ibid.*, **133**, 1350 (1986).
4. F. J. Nuzzi, *Plat. Surf. Fin.*, **70**, 51 (1983).
5. M. Paunovic, *This Journal*, **124**, 349 (1977).
6. F. M. Donahue, D. J. Sajkowski, A. C. Bosio, and L. L. Schafer, *ibid.*, **129**, 717 (1982).
7. W. Goldie, *Plating*, **51**, 1069 (1964).
8. L. N. Schoenberg, *This Journal*, **118**, 1571 (1971).
9. K. Kondo, J. Ishikawa, O. Takenaka, T. Matsubara, and M. Irie, *ibid.*, **137**, 1859 (1990).
10. R. L. Meek, *ibid.*, **122**, 1177 (1975).
11. J. F. Fisher and J. L. Hall, *Anal. Chem.*, **39**, 1550 (1967).
12. J. M. Bolling and J. L. Hall, *J. Am. Chem. Soc.*, **75**, 3953 (1953).
13. D. J. Alner and M. A. A. Kahn, *J. Chem. Soc.*, 5265 (1964).
14. A. Nozaki and M. Demori, *Nippon Kagaku Zasshi*, **84**, 42 (1963).
15. G. S. Smith and J. L. Hoard, *J. Am. Chem. Soc.*, **81**, 556 (1959).
16. J. L. Hall, F. R. Jones, C. E. Delchamps, and C. W. Mcwilliams, *ibid.*, **79**, 3361 (1957).
17. K. H. Pearson and K. H. Gayer, *Inorg. Chem.*, **3**, 476 (1964).
18. A. Molenaar, M. F. E. Holdrinet, and L. K. H. van Beek, *Plating*, **61**, 238 (1974).

The Effect of Chromium Particles on Nickel Electrodeposition

Sandra W. Watson* and Richard P. Walters*

U.S. Bureau of Mines, Albany Research Center, Albany, Oregon 97321

ABSTRACT

In order to obtain an understanding of the mechanism of chromium particle occlusion in electrodeposited stainless-steel-type coatings, the U.S. Bureau of Mines has studied the effect of chromium particles on nickel electrodeposition. The chromium particles catalyzed nickel electrodeposition on a vitreous carbon surface. Chromium particle additions, when added to Watt's-type electrolytes, of 0.33*M*, 0.67*M*, and 1.00*M* $NiSO_4$, shifted the nickel reduction wave to more positive potentials on a vitreous carbon surface. From rotating cylinder electrode studies it was concluded that nickel deposition with or without chromium particles is a kinetically limited rather than mass-transfer-limited process. Electrochemical impedance spectroscopy experiments with and without chromium particles verified the rate-determining step proposed by Epelboin, with the $Ni^+(ads)$ limiting the nickel electrodeposition. The chromium particles appear to enhance the formation of this $Ni^+_{(ads)}$ intermediate.

Insoluble particles suspended in an electrolyte during plating can be occluded in an electrodeposited coating (1-3). The Bureau of Mines has been successful in producing stainless steel coatings on low-alloy steel substrates by heat-treating an electrodeposited binary alloy of nickel and iron with occluded chromium particles (4-6). As a first step in understanding the mechanism of this particle occlusion, the effect of chromium particles on nickel electrodeposition has been studied.

Previous studies by Bazzard and Boden (7) concluded that chromium particle occlusion occurs as a result of collisions of the particles with the cathode surface. The changes Bazzard and Boden observed in the polarization behavior and increased current at a fixed potential were attributed to the increased surface area due to the particles and an increased surface ion activity. The latter effect resulted from fresh solution brought to the surface by the stationary film of liquid on each particle. Bazzard and Boden also considered the effect of having conductive chromium particles within the electric field. Due to the small size of the particles, substantial polarization of them did not occur. However, a local anode and cathode were set up on each particle in accordance with its position in the electric field. The conductive chromium particle affected the electric field gradient as it approached the cathode, resulting in a local rise of the current of the cathode. This local rise in current ensured rapid incorporation of the chromium particle. However, no large-scale electrophoretic or electrochemical effect was involved in the particle occlusion process, according to Bazzard and Boden. This study sought to examine the effect of the chromium particles on the mechanism of nickel deposition from a sulfate electrolyte during the occlusion process.

Experimental

All research was conducted in a three-electrode, modified Greene cell with a volume of 1000 ml. The experimental cell resided in a temperature-controlled water bath regulated at 70°C. The experimental cell was purged with nitrogen gas prior to the experiments. A small rod of vitreous carbon embedded in glass with an exposed surface area of 0.08 cm^2 was used as the stationary working electrode (cathode) for the slow sweep studies, while a rotating cylinder electrode of vitreous carbon (0.665 cm^2 surface

* Electrochemical Society Active Member.

area) was used for the rotating cylinder and electrochemical impedance spectroscopy (EIS) studies. The reference electrode was a saturated calomel electrode (SCE) connected to the Greene cell by a Luggin probe assembly. An inert counterelectrode of graphite rod, generating H^+ as its product at the anode (the anodic reaction was the breakdown of H_2O to form H^+ and O_2), was used. Therefore, the potentiostatic scans were limited to a region (−0.45 to −0.85 V SCE) where the pH (approximately 4) did not change during experiments.

Electrolytes were composed of nickel sulfate, enough sodium sulfate to maintain the sulfate ion concentration constant at 1*M*, and 0.65*M* boric acid. Commercially available chromium powder (>99% Cr) was used in this study. The particles were of a spherical shape with a size distribution of 0.3 to 60 μm diam; the majority of the particles were 1-2 μm in diam as determined by image analysis on a scanning electron microscope. Slow-sweep polarization studies of nickel electrolytes at three concentrations of $NiSO_4$, 0.33*M*, 0.67*M*, and 1.00*M*, with the addition of 0.1 and 4.2 volume percent (v/o) chromium particles, were conducted. (When a tenfold increase from 0.1 v/o to 1 v/o did not show a clear trend in 0.33*M* $NiSO_4$ electrolyte, a 40 to 50-fold increase was tried. A good suspension of the particles in the electrolyte was obtained at 4.2 v/o.) The electrolyte concentration of 0.67*M* $NiSO_4$ with and without 4.2 v/o chromium particle additions was used for the rotating cylinder electrode and EIS studies. The rotating cylinder experiments were conducted at rotation rates of 500, 1000, 1500, and 2000 rpm. Some EIS experiments were also conducted at room temperature.

The slow potentiodynamic polarizations, sweep rates of 1 mV/s, were performed with a PAR[1] Model 371 potentiostat, PAR Model 175 universal programmer, Fluke multimeter, HP computers, and in-house software. Impedance spectra were acquired in the frequency range of 100 kHz to 5 mHz with a rms peak value of 10 mV using a Solartron 1286 electrochemical interface, Solartron 1255 HF frequency response analyzer, a HP computer, and "ACDRIVE"[2] software. Impedance data were taken under potentiostatic control at −0.4, −0.6, −0.7, and −0.8 V SCE.

Results and Discussion

Slow sweep curves.—On the small vitreous carbon electrode the full forward scan beginning at 0 to −1.5 V SCE exhibited a limited current region (near −0.7 V SCE) followed by hydrogen reduction (Fig. 1). The addition of chromium particles affected the shape of the nickel reduction wave (increasing the length of the limited current region) for some of the concentrations of nickel electrolyte, and displaced the wave to more positive potentials for all of the concentrations. The positive displacement (depolarization) was greater for 4.2 v/o chromium than that for 0.1 v/o chromium. The greatest displacement occurred for 1*M* $NiSO_4$ containing a 4.2 v/o addition of chromium particles, as Table I indicates.

[1] Reference to specific trade names is made for identification only and does not imply endorsement by the Bureau of Mines.
[2] Purchased from Dr. Peter Searson, The Johns Hopkins University.

Table I. Nickel reduction wave displacement with addition of Cr particles.

Ni concentration *M*/l	Reduction wave displacement mV	
	Volume percent Cr	
	0.1	4.2
0.33	50	100
0.67	55	110
1.00	70	150

These trends also have been observed by M. Metzger and H. H. Tombrink (8) in their studies on the addition of SiC and colloidal graphite particles to a nickel sulfamate electrolyte. The shifts in reduction potentials were attributed to an increase in the active surface area by the adsorbed particles on the cathode. Metzger and Tombrink reported no change in the form of the reduction wave, only a potential displacement. Figure 2 shows an example of the results obtained during this study on the forward scans in the limited current region (−0.45 to 0.85 V SCE), which were in agreement with Metzger and Tombrink. The major shifts in reduction potential were only observed during the nucleation of the nickel deposit onto the foreign substrate (forward scan only). However, reverse scans, Fig. 3, exhibit no shift in the reduction potentials but do show increases in the current. Once a Ni deposit was formed and growing (reverse scan), the particles did not cause any further significant shifts in reduction potential. These results are consistent with the suggestion by Bazzard and Boden (7) that the concentration of nickel ions near the cathode is increased as the particles approach the cathode. Each collision of the particle with the cathode has the effect of momentarily increasing both the surface area of the cathode and the nickel activity at the surface.

Rotating cylinder electrode studies.—In general, the presence of chromium particles increased the limiting current during nucleation at all rotation rates (ω). Direct comparison to data with the stationary electrode was not possible, since the poor reproducibility of the rotating electrode was believed to be caused by the heterogeneous nature of the reduction reaction. The observed limiting current plotted *vs.* $\omega^{2/3}$ did not produce a straight line, indicating that the limiting current was independent of mass transport at rotation rates from 500 to 2000 rpm. These results are consistent with rotating ring-disk electrode studies of Andricacos *et al.* (9), who concluded that agitation does not affect the nickel deposition reaction. For the Andricacos

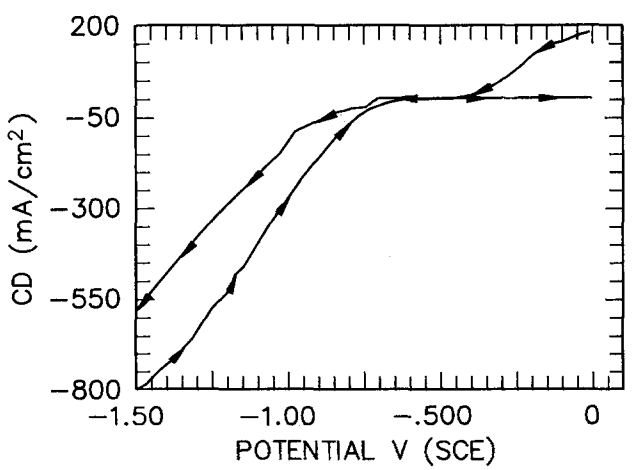

Fig. 1. Full forward and reverse scans of nickel electrodeposition without chromium particles from 0.67*M* $NiSO_4$ electrolyte.

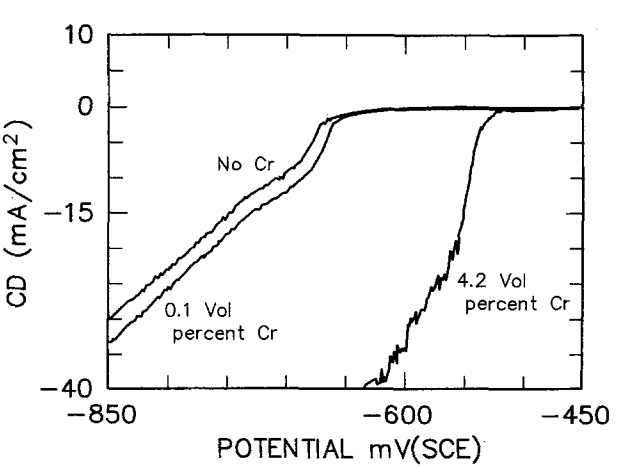

Fig. 2. Limited forward scans of nickel electrodeposition with chromium particle additions from 1*M* $NiSO_4$ electrolyte.

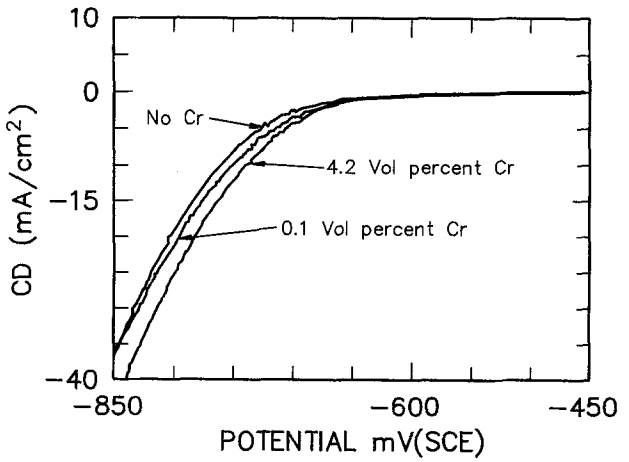

Fig. 3. Limited reverse scans of nickel electrodeposition with chromium particle additions from 1M $NiSO_4$ electrolyte.

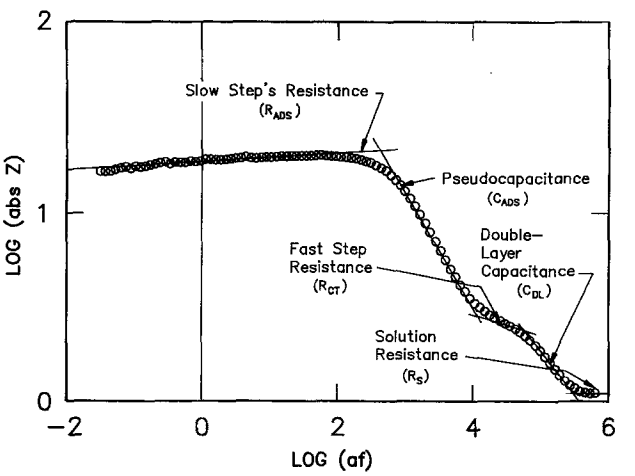

Fig. 5. Typical Bode plot of EIS displaying resistance and capacitance components.

data a plot of log Ni current density *vs.* electrode potential for data collected at 100 and 1600 rpm coincided. Within the range of rotation rates for this Bureau of Mines study, it appears that the limiting current is related to a kinetic rate-determining step during nickel nucleation on the vitreous carbon surface.

EIS studies.—To further elucidate the effect of the chromium particles on the mechanism of nickel nucleation on a vitreous carbon surface and subsequent deposition of the nickel coating, EIS was performed. The shapes of all of our Bode plots are characteristic of a capacitor and resistor in parallel rather than in series. From our EIS studies we found nickel electrodeposition to be a multi-step reaction process involving first a charge transfer reaction, a surface-adsorbed intermediate produced by the charge transfer reaction, and the subsequent removal of the adsorbed intermediate by a second or possibly third reaction. The equivalent circuit which describes the electrical response of an electrochemical reaction with a strongly adsorbed intermediate is shown in Fig. 4. In this circuit R_s represents the solution resistance (including IR drop), R_{CT} is the charge transfer resistance, and C_{ADS} and R_{ADS} are components that contain the contribution of surface coverage of the adsorbed intermediate and the rate of desorption. These electrical responses for the electrochemical reaction can be extracted from the Bode plot. Beginning at the low-frequency end of the Bode plot (Fig. 5), the resistance of the slow, rate-determining step (R_{ADS}) is followed by the pseudocapacitances (C_{ADS}), fast step, charge transfer resistance (R_{CT}), and last the total resistance of the solution including IR drop (R_S).

A possible mechanism for this multi-step nickel electrodeposition from a sulfate electrolyte was first proposed by Epelboin *et al.* (10), with more discussion by Chassaing *et al.* (11). In our case at the higher pH of 4, steps [2]-[4] are the most likely reactions to be occurring. Steps [5]-[7] have been proposed to occur at low pH (pH of 1.5 to 3), where the $H^*_{(ads)}$ is strongly bonded to the surface and acts as an inhibitor for hydrogen evolution. The Epelboin mechanism gives a very simplistic description of this hydrogen evolution reaction on the coated Ni surface (reactions [1] and [5]-[7]). A more descriptive mechanism of proton discharge followed by rate-determining electrodic desorption is given by Kobosew and Nekrassow (12).

Epelboin *et al.* mechanism

$$2H^+ + 2e^- \rightarrow H_2 \quad [1]$$

$$Ni^{+2} + e^- \rightarrow Ni^+_{(ads)} \quad [2]$$

$$Ni^+_{(ads)} + e^- \rightarrow Ni^\circ \quad [3]$$

$$Ni^+_{(ads)} + Ni^{+2} + 2e^- \rightarrow Ni^\circ + Ni^+_{(ads)} \quad [4]$$

$$Ni^+_{(ads)} + H^+ + e^- \rightarrow Ni^+_{(ads)} + H^*_{(ads)} \quad [5]$$

$$2H^*_{(ads)} \rightarrow H_2 \quad [6]$$

$$Ni^+_{(ads)} + H^*_{(ads)} + e^- \rightarrow Ni + H_{(included)} \quad [7]$$

The $Ni^+_{(ads)}$ species, probably a hydroxide or an oxyhydroxide, plays a vital role in the Epelboin mechanism. Matulis and Slizys (13) also report that nickel deposits from a $NiOH^+$ ion species in the pH range of 4.0 to 4.2. The EIS and slow sweep data from this research support the Epelboin mechanism. The Nyquist plots, with and without chromium particles, displayed the two inductive loops (shown in Fig. 6) mentioned by Epelboin and Wiart (14). The Nyquist plots demonstrated that two successive electron transfer reactions occurred during nickel reduction regardless of the presence of the chromium particles. Also, the variation of log of current with log of nickel concentration for the slow sweep data is first-order in nickel

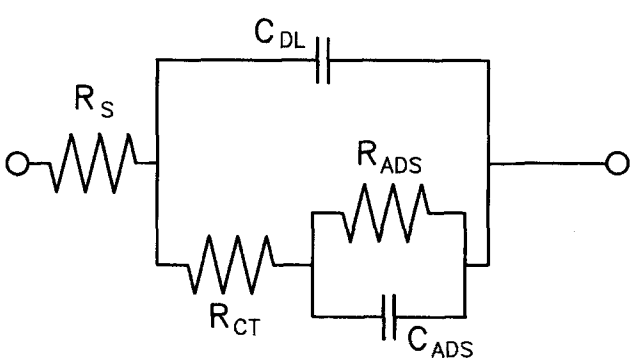

Fig. 4. An equivalent circuit which describes the electrical response of the electrochemical reaction for nickel electrodeposition.

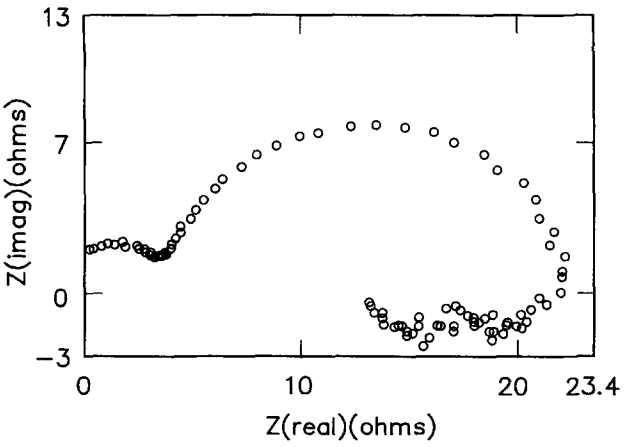

Fig. 6. Nyquist plot showing two inductive loops.

Table II. Pseudocapacitances.

Potentiostated potential (V SCE)	Temperature (°C)	Pseudo-capacitance w/o Cr particles ($\mu F/cm^2$)	Pseudo-capacitance w/Cr particles ($\mu F/cm^2$)
−0.4	70	486	186
−0.6	70	377	126
−0.7	70	83	100
−0.8	70	83	84
−0.7	31	313	NM
−0.8	31	166	NM
−0.4	24	NM	515
−0.7	24	NM	676

NM: Not measured.

Table III. Double-layer capacitance.

Potential, (V SCE)	Double-layer capacitance without Cr particles ($\mu F/cm^2$)	Double-layer capacitance with Cr particles ($\mu F/cm^2$)
−0.4	4.4	2.1
−0.6	4.2	2.3
−0.7	3.6	2.1
−0.8	3.7	2.5

concentration, suggesting that the Ni^{+2} is reduced one electron at a time.

The pseudocapacitance was interpreted as a measure of the adsorbed intermediate $Ni^{+}_{(ads)}$. The pseudocapacitances calculated from the Bode plots are shown in Table II. The pseudocapacitance is determined by extending the slopes for the pseudocapacitance and slow step resistances until the slopes cross; the cutoff frequency and resistance are determined at this crossover point. The pseudocapacitance is the reciprocal of the product of cutoff frequency and resistance. The pseudocapacitance was also very temperature-dependent; note the elevated values at the lower temperature. The temperature dependence of these capacitance values clearly shows that these capacitances are pseudocapacitances. Pseudocapacitance is temperature-dependent, whereas double-layer capacitance is not temperature-dependent. The double-layer capacitance values at the lower temperatures were the same as the values at 70°C.

Comparisons of the Bode plots at the various potentials, both with and without chromium particles, indicated that at the same potential, *viz.*, −0.4 V SCE, the pseudocapacitance appeared more pronounced when the chromium particles were not present. The pseudocapacitances of Table II support this observation. The pseudocapacitance values are larger without chromium particles at potentials prior to the nickel electrodeposition at −0.7 V SCE. After the adsorbed intermediate is formed on the substrate to establish the slow rate-determining step, the nickel deposition can proceed. Thus, the pseudocapacitance values become equivalent for either case, with or without chromium particles, at approximately −0.7 V SCE. The role of the chromium particles therefore was to reduce the potential required for the establishment of the surface adsorbed species.

Whether the chromium particles were delivering more metallic ions or more adsorbed intermediate cannot be determined. However, if the corrosion proposed by Bazzard and Boden (7) occurred on the chromium particles, then there is a possibility of nickel reduction on the particle surfaces in solution. Although no unambiguous evidence exists of nickel plating on the chromium particles in solution, analyses of particles remaining in the electrolyte after extensive plating indicate the presence of nickel on the particles.

Double-layer capacitance.—The double-layer capacitance values tabulated in Table III were calculated from the slope of a plot of angular frequency *vs.* imaginary admittance rather than from the Bode plots because of precision. The order of magnitude for double-layer capacitance values was checked and confirmed by a Bode plot calculation. These double-layer capacitance values are one order of magnitude smaller than values previously reported by other researchers (10-16). Volk and Fischer (15) reported a double-layer capacitance value of 50 $\mu F/cm^2$ at 25°C using oscillographic measurement of the ohmic drop after switching the current on; Kruglikov *et al.* (16) derived a value of 60 $\mu F/cm^2$ at 30°C using a potential decay method; and Epelboin and Wiart (14) calculated a value of 70 $\mu F/cm^2$ by a least squares method from the elements of a representative circuit to fit impedance experimental data measured at 30°C.

In order to investigate the apparent differences between our results and the above-mentioned literature values, Epelboin's Nyquist plots were digitized and analyzed with our "ACDRIVE" software. Our analyses indicate that Epelboin's double-layer capacitance corresponds, both in frequency range and magnitude, to our pseudocapacitance region. We were not able to determine double-layer capacitance values from Epelboin's data due to lack of high-frequency data. Perhaps the current technology of direct calculation of double-layer capacitance from impedance data gives a more precise value than transient techniques with many assumptions and the use of slower responding oscilloscopes employed by the researchers in the 1960s. Regardless of the cause, we believe that previous results for double-layer capacitance values for nickel reduction via the adsorbed intermediate mechanism reflect the pseudocapacitance associated with the adsorption of the intermediate.

There appears to be a weak potential dependence of the double-layer capacitance without chromium particles, whereas the double-layer values with Cr particles have no potential dependence. The double-layer capacitance is probably potential-independent in the presence of chromium particles because of the excess Ni^{+2} and/or $Ni^{+}_{(ads)}$ provided to the surface over the entire potential range studied.

Time constants.—The slope of a plot of the product of imaginary impedance x angular frequency *vs.* real impedance yields the time constants of a reaction step, and the y intercept is equivalent to the resistance for this reaction step. The time constant data with and without chromium particles are tabulated in Tables IV and V. The time constant analysis clearly indicated the positive potential shift in the reduction mechanism. The more defined time constants (time constant value does not change with potential)

Table IV. Time constant data without Cr particles.

Potentiostated potential (V SCE)	Step time constant (s)	Step resistance (Ω-cm^2)	Slower step time constant (s)	Slower step resistance (Ω-cm^2)	Slowest step time constant (s)	Slowest step resistance (Ω-cm^2)
−0.4	NA	NA	NA	NA	NA	NA
−0.6	7.6×10^{-6}	2.3	NA	NA	NA	NA
−0.7	9.3×10^{-6}	2.8	1.1×10^{-3}	19.6	NA	NA
−0.8	9.8×10^{-6}	2.6	1.6×10^{-6}	6.2	NA	NA

NA: data are not obtainable from the graph.

Table V. Time constant data with Cr particles.

Potentiostated potential (V SCE)	Step time constant (s)	Step resistance (Ω-cm^2)	Slower step time constant (s)	Slower step resistance (Ω-cm^2)	Slowest step time constant (s)	Slowest step resistance (Ω-cm^2)
−0.4	1.8×19^{-4}	11.5	NA	NA	NA	NA
−0.6	8.5×10^{-6}	3.5	1.6×10^{-3}	49.5	NA	NA
−0.7	9.1×10^{-6}	3.4	1.7×10^{-3}	12.4	0.9	15
−0.8	8.7×10^{-6}	3.3	1.7×10^{-3}	7.5	0.7	7.3

NA: data are not obtainable from the graph.

suggest that the chromium particles were catalyzing the nickel electrodeposition by enhancing the formation of the $Ni^+_{(ads)}$ intermediate. With Cr particles, the time constant value for the first (fastest) step was approximately 9×10^{-6} s, and 1.7×10^{-3} s for the slower step for all potentiostated potentials of −0.6, −0.7, and −0.8 V SCE. On the other hand, without Cr only the first step was defined at 9.3×10^{-6} to 9.8×10^{-6} s for potentiostated potentials of −0.7 and −0.8 V SCE; the slower time constant was not independent of potential. These results suggest that the chromium particles were catalyzing these slower steps. Perhaps this slowest step, only defined when chromium particles were present, at potentiostated potentials of −0.7 and −0.8 V SCE involves a $H^*_{(ads)}$ species as well as $Ni^+_{(ads)}$ in reactions such as steps [5]-[7] in the Epelboin (10, 11, 14) mechanism or Kobosew and Nekrassow (12) mechanism.

Conclusions

In conclusion, with or without chromium particles, nickel electrodeposition is kinetically limited rather than mass-transfer-limited. All results support the mechanism proposed by Epelboin *et al.* in which the Ni^{+2} is reduced one electron at a time and the $Ni^+_{(ads)}$ intermediate limits the nickel electrodeposition. Chromium particles catalyze nickel deposition onto a foreign substrate. Chromium particles appear to enhance the formation of a $Ni^+_{(ads)}$ intermediate. The chromium particles could be acting as an additional surface site for the $Ni^+_{(ads)}$ intermediate to form, or providing an increase in the Ni^{+2} concentration at the surface, or delivering the $Ni^+_{(ads)}$ intermediate to the surface.

Manuscript submitted March 14, 1991; revised manuscript received June 25, 1991. This was Paper 361 presented at the Seattle, WA Meeting of the Society, Oct. 14-19, 1991.

The U.S Bureau of Mines assisted in meeting the publication costs of this article.

REFERENCES

1. J. C. Withers, Wadd Tech. Rep., 60-715 (1961).
2. T. W. Tomaszewski, R. J. Clauss, and H. Brown, *Tech. Proc. Am. Electroplater's Soc.*, **50,** 169 (1963).
3. T. W. Tomaszewski, L. C. Tomaszewski, and H. Brown, *Plating*, **56,** 1234 (1969).
4. J. E. Allison and G. R. Smith, *Tech. Proc. Am. Electroplater's Soc.*, **71,** 1 (1984).
5. G. R. Smith and J. E. Allison, U.S. Pat. 4,601,795 (1986).
6. J. E. Allison and G. R. Smith, BuMines RI 9213, 13 (1989).
7. R. Bazzard and P. J. Boden, *Trans. Inst. Metal Finish*, **50,** 63-69 (1972).
8. W. Metzger and H. H. Tombrink, 8th Congress of the International Union for Electrodeposition and Surface Finishing, 66-77 (1972).
9. P. C. Andricacos, C. Arana, J. Tabib, J. Dukovic, and L. T. Romankiw, *This Journal*, **136,** 1336 (1989).
10. I. Epelboin, M. Joussellin, and R. Wiart, *J. Electroanal. Chem.*, **119,** 61 (1981).
11. E. Chassaing, M. Joussellin, and R. Wiart, *ibid.*, **157,** 75 (1983).
12. N. I. Kobosew and N. Nekrassow, *Z. Electrochem.*, **36,** 529 (1930).
13. J. Matulis and R. Slizys, *Electrochim. Acta*, **9,** 1177 (1964).
14. I. Epelboin and R. Wiart, *This Journal*, **118,** 1577 (1971).
15. O. Volk and H. Fischer, *Electrochim. Acta*, **4,** 251 (1961).
16. S. S. Kruglikov, N. T. Kudryavtsev, and R. P. Sobolev, *Electrochim. Acta*, **12,** 1263 (1967).

On the Electronic Conduction in Dry Thin Films of Prussian Blue, Prussian Yellow, and Everitt's Salt

Anthony Xidis and Vernon D. Neff

Department of Chemistry and the Liquid Crystal Institute, Kent State University, Kent, Ohio 44242

ABSTRACT

Electron conductivities are reported for dry thin films of Prussian blue and its completely oxidized and reduced forms, Prussian yellow and Everitt's salt. It has been discovered that desiccated Prussian blue films are non-ohmic in the sense that significant electron conduction does not occur below a threshold voltage of *ca.* ± 0.5 V. Prussian yellow and Everitt's salt are ohmic and do not have a conduction threshold. The conductivities, as determined from the slopes of the *i-V* curves, are essentially the same for Prussian yellow, Everitt's salt, and Prussian blue above the voltage threshold, and are *ca.* 5×10^{-7} $(\Omega\ cm)^{-1}$. The solid state voltammogram of a wet film is also considered in terms of the persistence of the threshold and the onset of electrochemistry. We propose a qualitative explanation for the threshold voltage based on the assumption that the "valence band" (ferric ferrocyanide) is completely occupied and that the applied voltage injects electrons into the "conduction band" (ferrous ferricyanide).

Since the classic discussion of Robin and Day on mixed valence crystals, Prussian blue has been regarded as the prototype example of a mixed-valence transition metal hexacyanide (1). During the past decade, following the discovery of the electrochemical activity of Prussian blue and related hexacyanides, there has been considerable interest in the electronic and ionic conductivity of this class of compounds. Under conditions where ionic transport is facilitated, as with thin films of Prussian blue (ferric ferrocyanide or PB) in aqueous potassium ion solutions, it is